Available online at www.derpharmachemica.com

ISSN 0975-413X
CODEN (USA): PCHHAX

Der Pharma Chemica, 2017, 9(5):79-91
(http://www.derpharmachemica.com/archive.html)

Adsorption Behaviour of *Vitex doniana* on Annealed Carbon Steel Corrosion in Hydrochloric Acid: Experimental and Theoretical investigations

Oguike RS[1,2*], Omizegba FI, Oni O, Akanang H, Shibdawa AM

[1]*Department of Chemistry, Corrosion Protection and Materials Science Laboratory, Abubakar Tafawa Balewa University, Bauchi, Nigeria*
[2]*Department of Chemistry, Electrochemistry and Materials Science Research Laboratory, Federal University of Technology, Owerri, Nigeria*

ABSTRACT

The Interfacial activity of Vitex doniana (VD) leaves extract as inhibitor has been studied on carbon steel corrosion in hydrochloric acid solution using weight loss, gasometry, electrochemical techniques and quantum chemical calculations. Increase in inhibition efficiency with increased inhibitor concentration which indicate that VD molecules acted by accumulating at metal/electrolyte interface. Weight loss results show that inhibition efficiency increased with increase in inhibitor concentration but decreased with increase in temperature indicating a physical adsorption. Data obtained from the potentiodynamic polarization scan revealed that the corrosion inhibitor shifted corrosion potentials to more negative potential indicating prominent cathodic protection. The impedance data showed a decrease in double layer capacitance and an increase in charge transfer resistance which suggests that electron migration was retarded in the bulk solution. The Nyquist and Bode plots of the test solutions were similar in both inhibited and free medium but contained capacitive and inductive loops. To assess the interaction of VD molecules with Fe(110) surface, quantum chemical calculations were performed to elucidate the molecular reactivity parameters of inhibitor molecules while molecular dynamics studied the binding properties of inhibitor molecules on metal surface. Local reactivity was estimated and discussed through condensed Fukui indices. Theoretical calculations were carried out using Dmol3 basis set for all atoms.

Keywords: Annealed carbon steel, *Vitex doniana*, Density functional theory, Molecular dynamics, Corrosion inhibition

INTRODUCTION

The interfacial behavior of organic compounds at metal/electrolyte interface relates to electrochemical energy conversion, electro-organic synthesis, as well as corrosion inhibition which have aided in the search for better corrosion inhibitors [1]. The low corrosion resistance of pure carbon steel is due to its incapacity to build up a protective oxide layer on its surface that contains the changing chemistry of attacks by corrosive environments, but inhibitors are paramount in such cases of corrosion prevention. Carbon steel can safely be operated in very corrosive service conditions if corrosion control systems are properly designed and implemented. Some industrial divisions such as acid pickling, descaling processes, pipelines, chemical operation units, steam generators, oil and gas production units are all involved with inhibitors due to high corrosion rates in its process [2]. Several authors have reported on the use of eco-friendly inhibitors to mitigate corrosion of carbon steel, mild steel, stainless steel, aluminium, magnesium and many other metal/alloys in both acid and alkaline solutions [3-7].

The choice of potential corrosion inhibitor takes into consideration the geometric and electronic properties of the molecular compound while other parameters such as environmental characteristics, nature of the metal and other experimental conditions also play important roles. Many authors believe that corrosion inhibitor efficiency basically point to their molecular structure [8-12] while the presence of unique atoms such as N, O and S in heterocyclic compounds has been widely reported to be an effective factor that enhances protection efficiency of inhibitors in corrosive media [13-17]. The geometry of the molecule has strong influence in the adsorption behaviour of inhibitor molecule on metal surface, via predicting the best possible orientation by which the inhibitor molecule covers the metal surface. Moreover, the electronic parameter informs about the molecules' tendency to react through electrons donor/acceptor bonds and as such binds on metal surfaces. Interfacial interaction between the inhibitor molecule and metal surface depends strongly on the electron density distribution of the inhibitor molecule. Adsorption of inhibitor molecule is expected to be all over the metal surface with the resultant adsorbed layer functioning as a barrier which prevents further corrosion of the metal [17]. Studies to obtain effective eco-friendly, cheap and renewable corrosion inhibitor is continuing with increasing number of plants explored for their corrosion inhibition potentials. *Vitex doniana* commonly known as African black plum is a perennial tree whose leaves are used for medicinal purposes. Ladeji and Okoye [18] studied the ability of an aqueous extract of *V. doniana* to protect the liver of albino rats from carbon tetrachloride-induced liver damage.

Chromatogram analysis of *V. doniana* leaves extract yielded constituents such as benzenepropanenitrile, 1,3-dimethoxy-2-hydroxybenzene, tripropylborane, 5-hydrxoymethylfurfural, 2-butene oxide, 1,3-butylene diacetate, methyl mandelate, pyrimidine-2,4(1H,3H)-dione, among others.

In addition to traditional techniques such as electrochemical, gravimetric and gasometry, quantum chemical calculation gives important physical insight on corrosion inhibition mechanism. Density Functional Theory (DFT) has been broadly used to analyze molecular electronic properties of adsorption-type inhibitors using a number of quantum chemical descriptors [19-21]. Literature has shown that inhibition efficiency is correlated to the molecular and structural reactivity parameters that can be obtained through theoretical calculations such as chemical selectivity, local reactivity and charge distribution [22]. Other quantum chemical results are the frontier molecular orbital; Higher Occupied Molecular Orbital Energy (HOMO), the Lower Unoccupied Molecular Orbital (LUMO) energy, chemical potential (μ) and hardness (η), electronegativity (χ) and electron transfer number (ΔN) among others [20,21]. In this study, we report the possible role of VD leaves extract as corrosion inhibition for FE164531 surface in aqueous hydrochloric acid solution using weight loss, gasometry, electrochemical techniques and quantum chemical calculations. Insight into the adsorption mechanism was assessed through electrochemical impedance spectroscopy (EIS) while the effect of temperature gave thermodynamic parameters such as ΔH_{ads} and ΔS_{ads}. Quantum chemical calculations were performed to evaluate molecular reactivity of VD molecules while molecular dynamics study was used to investigate the binding energy of individual VD molecule on Fe(110) surface. Six molecules selected from the chromatogram analysis based on geometric and electronic properties are namely; pyrimidine-2,4(1H,3H)-dione (PID), 4H-pyran-4-one (HPO), 2-furancarboxaldehyde (FCA), 2,6-dimethoxy-phenol (DOP), Benzenepropanenitrile (BPN) and benzeneacetic acid (BAA). Figure 1 below shows the Lewis structures of the investigated inhibitor molecules while their optimized geometric structures are presented in Figure 2.

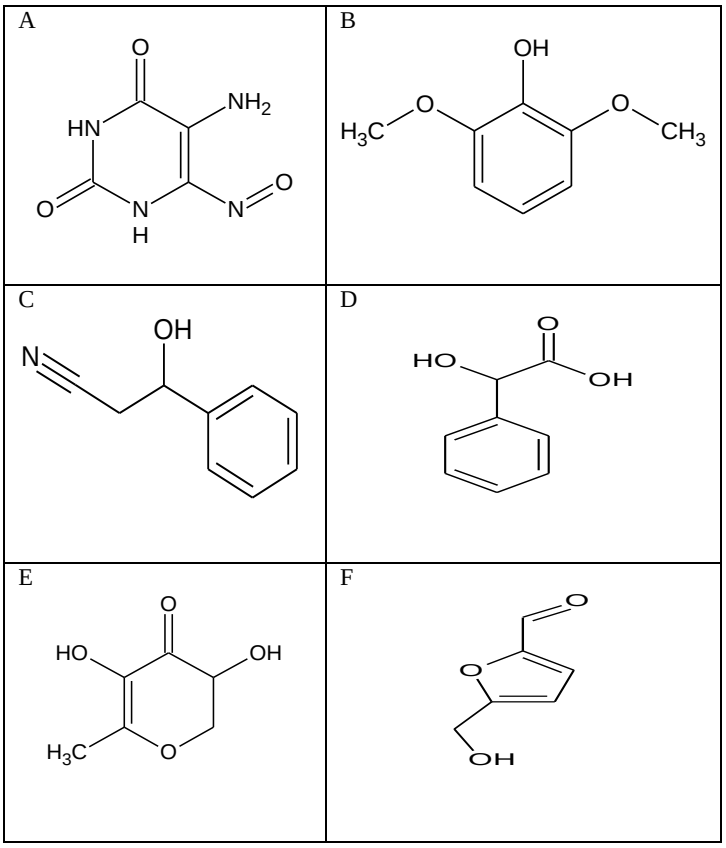

Figure 1: Lewis structures of the investigated inhibitor molecules showing name and abbreviation. (A) Pyrimidine-2,4(1H,3H)-dione (PID), (B) 2,6-Dimethoxy-Phenol (DOP), (C) Benzenepropanenitrile (BPN), (D) Benzeneacetic acid (BAA), (E) 4H-Pyran-4-one (HPO), (F) 2-Furancarboxaldehyde (FCA)

EXPERIMENTAL

Material preparation

Annealed carbon steel (FE164531) sheets of 99.5% purity, used for this study has the following typical analysis ppm: C<1200, Mn<5000, S<500, P<500 which was procured commercially from Advent research materials Ltd, Eynsham Oxford England OX29 4JA. The sheet was press-cut into suitable dimensions with a hole of 1mm drilled at the middle of the upper edge of the coupons and then abraded successively with metallographic emery paper of increasing fineness of up to 1200 grits. These coupons were degreased in absolute ethanol, dried in acetone, further dried with hot air and stored in moisture-free desiccator prior usage. Dried leaves of VD were blended to powder form; 50 g of powdered leaves was refluxed in 500 ml ethanol, allowed to cool for 3 h and filtered. The filtrate was concentrated using rotary evaporator and stored in an oven at 40°C.

From the concentrate, inhibitor test solutions were prepared in concentrations of 10, 100 and 1000 ppm. Part of the concentrate was taken for chromatogram analysis using a GCMS-QP2010 PLUS Shimadzu, Japan. All test solutions were freshly prepared from analytical grade chemical reagent using bidistilled water. Data analyses were carried out using Origin Pro 8 Data analysis station & graphing workspace.

Weight loss

In weight loss experiments, FE164531 coupons (4.0 × 4.0 × 0.92 mm) were weighed before total immersion in a 250 ml beaker containing 200 ml test solutions, being suspended by suitable hooks at 1 cm below the solution surface. The beakers were placed in a freely aerated thermostated water bath maintained at constant temperature at 303, 313, 323 and 333 ± 0.5 K. The coupons were retrieved after 3 h, scrubbed with brush under running bidistilled water, dried and weighed [23]. The difference in weight before and after immersion of the coupons in different test solution was taken as the weight loss. This was used to calculate the corrosion rate in millimeter penetration per year (mmy^{-1}) using Equation 1 [23].

$$K_{CR} = \frac{k\Delta W}{\rho AT} \quad (1)$$

where k=unit of corrosion rate constant (8.76×10^4 mmy^{-1}), ΔW is weight loss in mg, ρ is density of metal, T is exposure time in hours, A is area of working electrode. Inhibition efficiency (*%IE*) was calculated using the following expression Equation 2:

$$\%IE = \left(1 - \frac{K_{CR(inh)}}{K_{CR(blank)}}\right) x\ 100 \quad (2)$$

Where, $CR_{(inh)}$ and $CR_{(blank)}$ are the corrosion rate in the presence and absence of leaf extracts respectively.

Gasometric

One hundred milliliters of test solution poured into a reaction vessel was used in the gasometric method. Upon introduction of the metal coupon (4.0 × 2.0 × 0.92 mm), the vessel was quickly corked and the initial volume of air was recorded against the level of paraffin oil in the burette. A decrease in volume of the paraffin oil in the burette due to hydrogen gas evolution was noted after every five minutes till the last volume of paraffin oil in the burette. The volume of hydrogen gas evolved was used to evaluate inhibition efficiency of the test inhibitors using Equation 3 [24].

$$E_H\% = 1 - \frac{CR_H}{CR_H^0} \quad (3)$$

Where, CR_H and CR_H^0 are corrosion rates got from total volume of gas evolved in the presence and absence of test inhibitors respectively.

Electrochemical technique

The polarization and impedance studies were carried out using Potentiostat/Galvanostat model 263 using Power Suite software. Data were taken after the carbon steel with an exposed area of 1 cm^2 was immersed for 1800 sec in aerated test solution at open circuit potential. The potentiodynamic polarization curves were obtained by scanning the potential of carbon steel from −0.25 V to 1.6 V vs. SCE at a scan rate of 0.33 mV/s while impedance spectroscopy experiments (EIS) was scanned at the open-circuit potential at frequencies from 100 kHz to 0.1 Hz with AC signal amplitude of 5 mV peak-to-peak along phase shifts [17]. The Nyquist and bode plots were acquired using ZSimpWin Version 3.20 software. The values of E_{corr}, i_{corr}, R_t and C_{dl} were obtained from the electrochemical measurements. The corrosion inhibition efficiencies were determined using Equation 4 [17]:

$$E_i\% = \frac{i^\circ_{corr} - i_{corr}}{i^\circ_{corr}} \quad (4)$$

Where i_{corr} and i°_{corr} is corrosion current densities for inhibited and uninhibited solutions respectively.

Computations

All stimulations were done using MS Modeling 4.0 software (available from Accelrys, San Diego, CA, USA). The geometry optimization process was carried out for inhibitor molecules and the Fe surface by means of the DFT electronic structure program, DMol3 using a Mulliken population analysis as well as a Hirshfeld numerical integration procedure. Electronic parameters for the simulation include unrestricted spin polarization using the DNP basis set and local potential Perdew and Wang (PWC) exchange-correlation potential functional [15]. DFT Semi-core Pseudopots (DSPP) was used as the core treatment which replaces core electrons by a single effective potential. 2 × 2 × 1 mesh parameters was set as *k* point with custom grid for the metal surface and density mixing charge was set to default using Direct Inversion in an Iterative Subspace (DIIS) with 0.14 eV thermal smearing applied to the orbital occupation to speed up convergence alongside convergence tolerance maximum force at 0.05 eV/Å. Molecular Dynamics (MD) simulation of the interaction between single inhibitor molecule and Fe(110) surface was performed using Forcite quench molecular dynamics [17] to sample several different low energy configurations and identify the low-energy minima. The Fe surface was first relaxed via minimizing its energy by geometry optimization and then cleaved along the (110) plane. The symmetry was increased and its periodicity changed by constructing a supercell 12 × 10 with a vacuum height of 20 Å. This serves as a representative part of the interface that is devoid of arbitrary boundary effects. Calculations were carried out; using the condensed-phase optimized molecular potentials for atomistic simulation studies (COMPASS) force field and the Smart algorithm, in a simulation box 29.79 Å × 24.82 Å × 26.08 Å with periodic boundary conditions. Stimulation conditions include fixed energy (NVE ensemble) with initial temperature of 303 K at time step of 0.1 fs was employed while the system was quenched every 250 steps with convergence tolerance energy at 1.0^{-4} kcal/mol and displacement of 5.0 x 10^{-5} Å. The adsorption energy (E_{Bind}) was calculated using the relationship in Equation 5 [22];

$$E_{Bind} = E_{Fe-inhibitor} - (E_{Inh} + E_{Fe}) \quad (5)$$

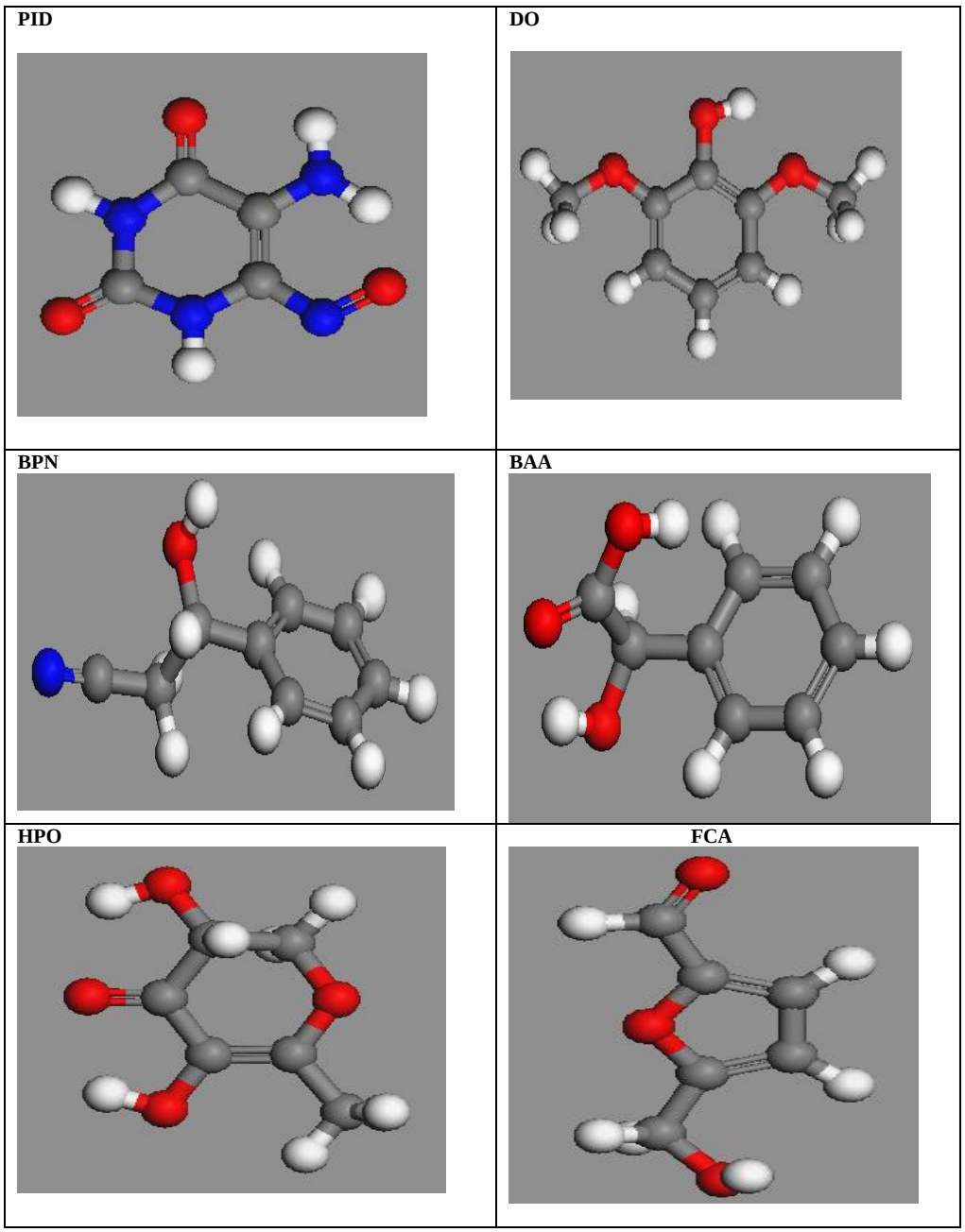

Figure 2: Geometry optimized structures of inhibitor molecules [C, gray; H, white; N, blue; O, red]

RESULTS AND DISCUSSION

Polarization measurements

The potentiodynamic polarization curves recorded for FE164531 electrode in 2 M HCl solution in the absence and presence different concentrations of VD leaves extract are presented in Figure 3. Electrochemical parameters such as corrosion potential (*Ecorr*) and corrosion current density (I_{corr}) shown in Table 1 were extracted using V3 Studio software. It was observed that both anodic and cathodic currents were reduced in the presence of with the reduction pronounced at the cathodic region. Corrosion potential values were found to shift towards the negative potentials with increasing inhibitor concentration. This effect indicates that the addition of VD leaves extract retards hydrogen evolution which is the main cathodic reaction of iron in acidic solutions. In acidic medium the reduction of H^+ ions at carbon steel surface takes place through a charge transfer mechanism [25]. The inhibitor molecule is presumed to adsorb on FE164531 surface thereby blocking available active sites from further corrosion reaction. In our study, FE164531 surface area available for H^+ ions reduction decreased without affecting the corrosion reaction mechanism; this agrees with the findings of Aljourani et al. [10]. Inspection of Figure 3 revealed that inhibition efficiency of VD leaves extract was concentration dependent with optimum protection at 1000 ppm (94%). The decrease in corrosion current density found at the anodic region suggests that the inhibitor reduced anodic dissolution via adsorption on FE164531 surface and simultaneously replaced preadsorbed water molecules on metal surface [17]. A compound can be classified as an anodic or a cathodic type inhibitor when the change in the corrosion potential value is larger than 85 mV [26]. As it can be seen, the displacement exhibited by VD leaves extract in the values of *Ecorr* are a bit greater than 85 mV hence, the consideration as cathodic type inhibitor.

This supports the observation from Figure 3, which shows a prominent I_{corr} decrease at the cathodic region. The protection effect of VD leaves extract might be in tune with the formation of a stable film comprising of γ-Fe_2O_3/Fe_3O_4 on FE164531 surface which slows down electron transfer in the redox process hence, a reduction of further corrosion across the metal surface.

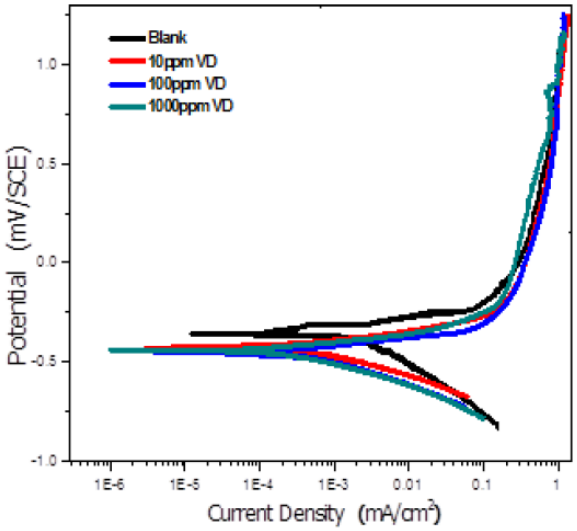

Figure 3: Anodic and cathodic polarization curves for FE164531 electrode in aerated solution of 2 M HCl in the absence and presence of different concentrations of VD leaves extracts

Impedance spectroscopy measurements

Impedance spectrum relate to the momentary behaviour of specific electrochemical interface with its dialectic behavior as well as oxidation–reduction reactions and migrations along the electrochemical interface [8]. These properties depend on homogeneity of the material surface and the electro-chemical properties of the service environment. Figure 4 show the Nyquist plot while obtained electrochemical parameters are presented in Table 1. The Nyquist plot displayed one capacitive loop of extended semicircle in the complex impedance plane both in uninhibited and inhibited solution. This is an indication that corrosion reaction is controlled by charge transfer resistance. The impedance diagrams obtained were not perfect semicircles which increased in diameter as inhibitor concentration increased; an indication that the presence of inhibitor molecules strengthens the surface film formation and/or the Faradic processes occurring through defects of this film was increased with VD leaves extract introduction. Inhomogeneities on the electrode surface was attributed the cause for imperfect semicircles obtained in impedance studies. Rivera-Grau et al. [27] proposed three frequency regions in Bode diagrams which are the high, intermediate and low frequency regions in association with the electrolyte resistance, cell geometry, impedance of the conductors and the reference electrode.

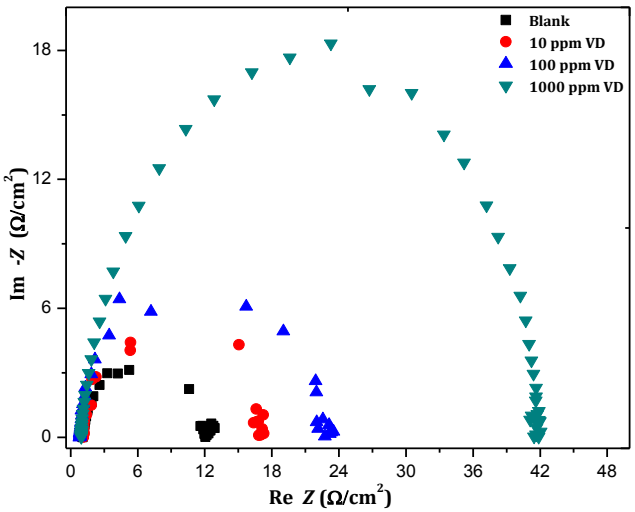

Figure 4: FE164531 carbon steel in 2 M HCl solutions with and without different concentrations of VD leaves extract

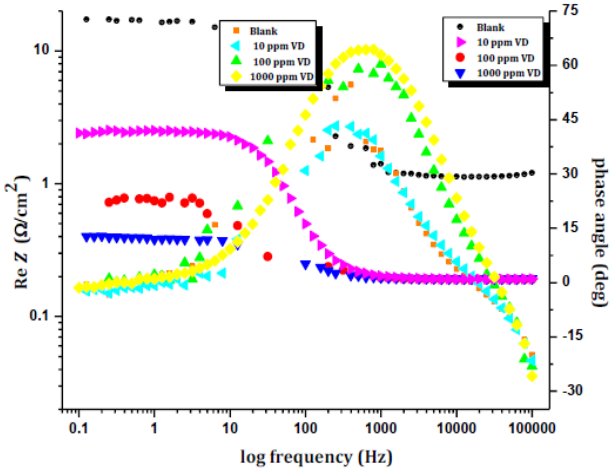

Figure 5: Bode plot of FE164531 carbon steel in 2 M HCl solutions with and without different concentrations of VD leaves extract

The Bode plot (Figure 5) is seen to exhibit an upland of the |*Z*| values in the high frequency region (*f*<10 kHz) as a response of the solution resistance (R_s) and double layer capacitance (C_{dl}) input. In the frequency region (*f*<10 Hz) a capacitive behavior is indicated from medium at low frequencies, suggesting an adsorbed film is formed on FE164531 carbon steel in 2 M HCl solutions. This effect propose a detection of electron charge transfer process or the mass transfer processes and/or other relaxation process taking place at the film–electrolyte interface which is presumed to occur within the pores of the surface film as the phase angle approach 69°. Nyquist complex plane plots obtained in this study shows one time constant corresponding to one capacitive loop, whose limits broadened in the presence of various concentration of VD leaves extract on account of formation of protective layers. This observation is also verified by the Bode plots, which shows a resistive region, defined with a horizontal line both at high and low frequencies. This factor points to the presence of compounds with hydrolysable functional groups in the leaf extract that can adsorb on the metal surface via lone pair of electrons. As a result, a barrier is formed on the metal surface which mitigates further corrosion attacks. The impedance data obtained were fitted into a Randles circuit which sufficiently explains EIS data for liquid and steam-treated samples [28]. Figure 6 show a typical Randles circuit consisting of solution resistance (R_s) in series with a component composed of transfer resistance (R_t) and parallel film capacitance (C_{dl}). A representative simulation of Nyquist and Bode diagrams with the equivalent model, in this case using 1000 ppm concentration of VD leaves extract for illustration is shown in Figure 7.

Table 1: Corrosion parameters obtained from temperature variation and polarization curves for FE164531 in 2 M HCl solution in the absence and presence of VD leaves extracts

	Parameters						
	i_{corr} (µA cm^{-2})	-E_{corr} (mV *vs.* SCE)	E_i %	R_t (Ω cm^{-2})	C_{dl} × 10^{-4} (µ cm^{-2})	ΔH^* (Jmol^{-1})	$-\Delta S^*$ (Jmol^{-1}.K)
Blank	5006.1	357.28	--	7.67	1.436	271.424	8.7864
10 ppm	2409.1	452.1	52	10.75	1.72	285.748	8.7443
100 ppm	834.99	458.79	83	21.18	0.568	308.338	8.6775
1000 ppm	326.45	453.9	94	39.55	0.438	375.127	8.4784

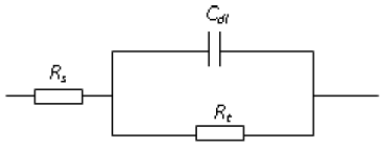

Figure 6: Electrical equivalent circuit used to fit the impendence data

The capacitance of parallel film (C_{dl}) was calculated from Helmholtz model (Eq. 6) which describes double layer capacitance as being inversely proportional to the surface film thickness Equation 6 [29];

$$C_{dl} = \frac{\varepsilon_o \varepsilon}{d} S \qquad (6)$$

Where ε_o is the permittivity of air, ε is the local dielectric constant, d is the film thickness, and S is the electrode surface. Table 1 show that C_{dl} values decreased when the concentration of the inhibitor molecules increased while R_t increased with concentration of the inhibitor. The decrease in C_{dl} might arise from a decrease in local dielectric constant and/or an increase of the electrical double layer thickness which might arise from substitution of preadsorbed water molecules at the metal/electrolyte interface by adsorbed VD leaves constituents whose dielectric constant is lower, signifying that VD molecules function via adsorption on metal surface [28-30]. Further, the decrease in active sites on the surface area available for corrosion may also be another reason for C_{dl} decreasing [29]. The increase in charge transfer resistance suggests that VD leaves extract actually retards migration of ions from the metal surface into the bulk solution which in turn, reduce further corrosion of the metal. This can be attributed to the slight modification of surface homogeneity due to inhibitor adsorption at most active corrosion sites.

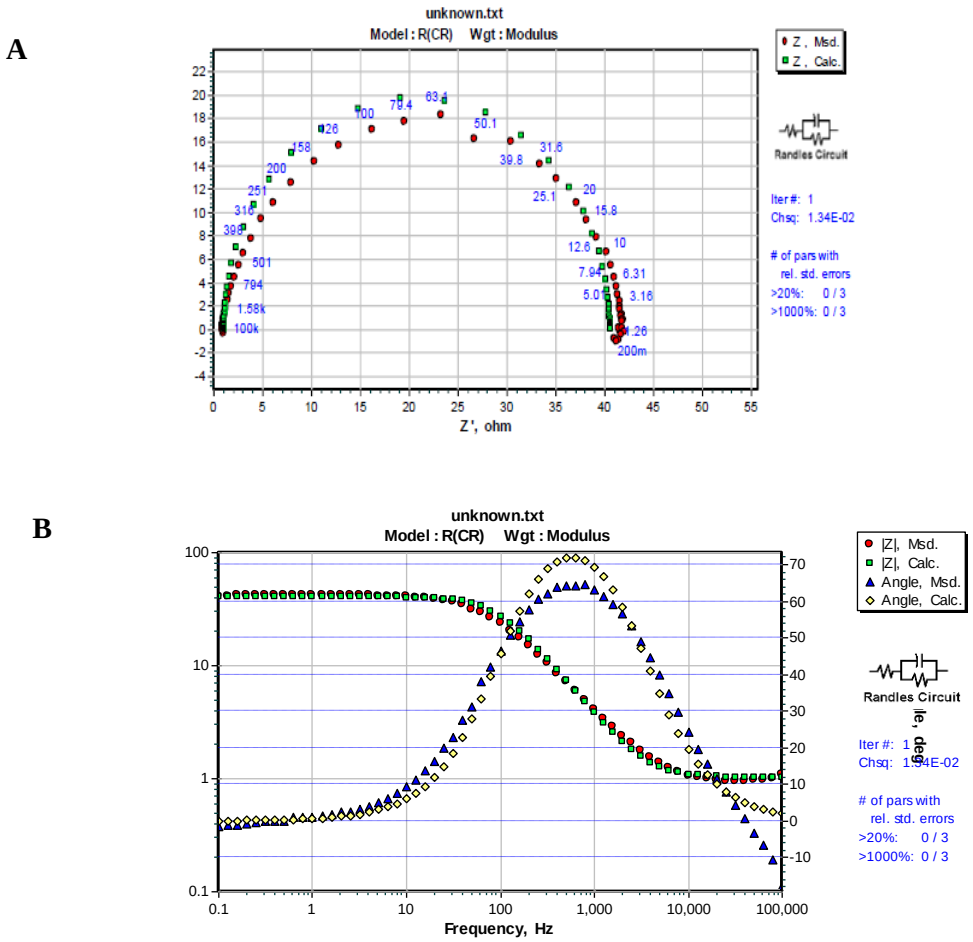

Figure 7: Simulation of Nyquist (A) and Bode (B) diagrams with 1000 ppm VD concentration data

Weight loss and gasometric technique

The gasometric technique ensures a more sensitive monitoring in situ of any perturbation by the inhibitor vis-a-vis hydrogen gas evolution on the metal-corrodent interphase [23]. The volume of H_2 evolved was observed to appreciably reduce in the presence of test inhibitors as compared to the free acid solution. Further reduction in the volume of H_2 evolved was observed as concentration of test inhibitor molecules increased. Figure 8 reveals that the most remarkable reduction in the volume of H_2 evolved was observed with VD molecules at 1000 ppm with inhibition efficiency of the inhibitor at 86%. The results obtained in the gasometric experiments are in agreement with the trend reported for electrochemical measurements. When the surface coverage of the adsorbed inhibitor species increases, lateral reactions between inhibitor molecules may arise, thereby influencing inhibition efficiency. Attractive lateral interactions usually give rise to stronger adsorption hence higher inhibition efficiency [31].

This effect has been shown in cases of compounds containing long chain hydrocarbon because of attractive Van der Waals forces. FE164531 was found to corrode at a substantial rate in 2 M HCl solution (Table 2). Results obtained clearly show that ethanolic extract of VD leaves effectively retards corrosion rate of FE164531 carbon steel in 2 M HCl solution. The weight loss data reveal the dependence of inhibition efficiency of VD on concentration and temperature. Figure 9 shows variation of FE164531 corrosion inhibition efficiency with temperature and inhibitor concentration. It is clear that increase in inhibitor molecules concentration for all tests performed at varying temperatures retarded corrosion reaction rate indicating geometric blocking effect at active corrosion sites [31,32]. Table 2 show results of corrosion rate and inhibition efficiency obtained from the weight loss experiment.

As observed, the corrosion rate increased with increase in temperature however, VD leaves extract is seen to decrease corrosion at all experimental temperatures. The increase in protection of the metal increased with increase in VD concentration suggesting that VD retards corrosion of Fe in HCl solution via adsorption with increased surface coverage on the metal as concentration increased. Decreased inhibition efficiency with temperature increase is often attributed to physical adsorption of the inhibiting species on the corroding metal surface [7]. This behaviour indicates that the VD functions better at low temperature with indications of desorption as temperature increases. Optimal inhibition efficiency (75%) was seen at 303 K with 1000 ppm VD concentration. Ita and Edem [32] suggested that the nitrogen/oxygen atom present in inhibitor molecules are easily protonated in acidic solution and are converted into quaternary/oxonium ions. These protonated species get adsorbed on the cathodic sites of the metal surface and decrease the hydrogen evolution hence retard metal dissolution. The results obtained from the weight loss experiment are in agreement with the data from hydrogen evolution experiment and electrochemical measurements.

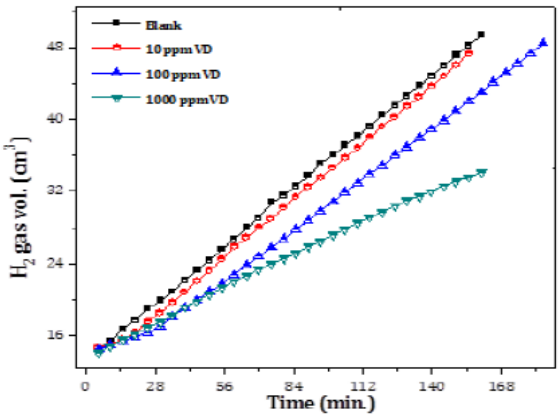

Figure 8: Variation of H_2 gas evolved with time for FE164531 carbon steel corrosion in 2 M HCl solutions with and without different concentrations of VD leaves extract

Table 2: Corrosion rate (mmy^{-1}) and inhibition efficiency (%IE) for Fe 1645 in 2 M HCl solution containing different concentrations of *Vitex doniana* (VD) at varying temperature (°K) determined by weight loss measurement

	303		313		323		333	
	K_{CR}	*%IE*	K_{CR}	*%IE*	K_{CR}	*%IE*	K_{CR}	*%IE*
Blank	168.3452	-	1998.0425	-	4385.4237	-	7767.7571	-
10 ppm	127.3963	24	1747.7997	12	4173.5298	05	7119.8952	08
100 ppm	87.7475	48	1437.1086	28	3717.2431	15	6594.0601	15
1000 ppm	41.5988	75	517.3851	74	3167.3582	28	6259.9697	19

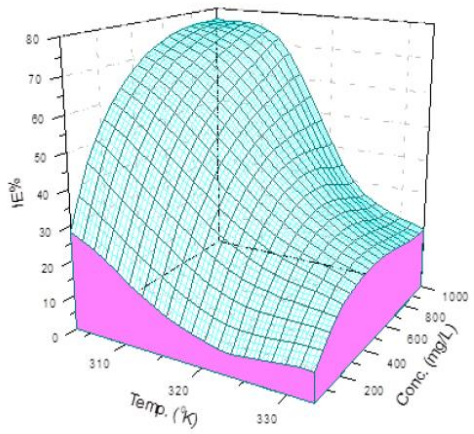

Figure 9: Corrosion inhibition efficiency of VD leaf extract as a function of temperature and inhibitor concentration for FE164531 in 2 M HCl obtained from weight loss

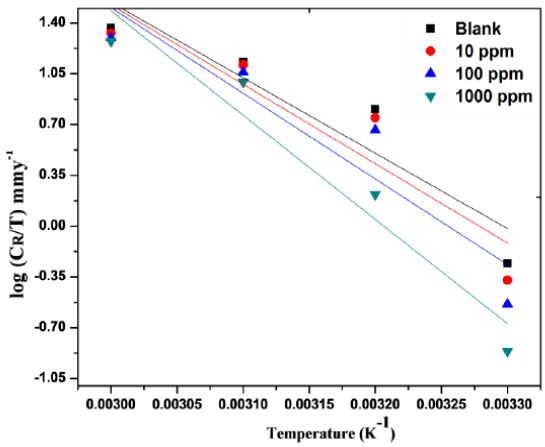

Figure 10: Transition state plot of FE164531 in 2 M HCl as a function of temperature

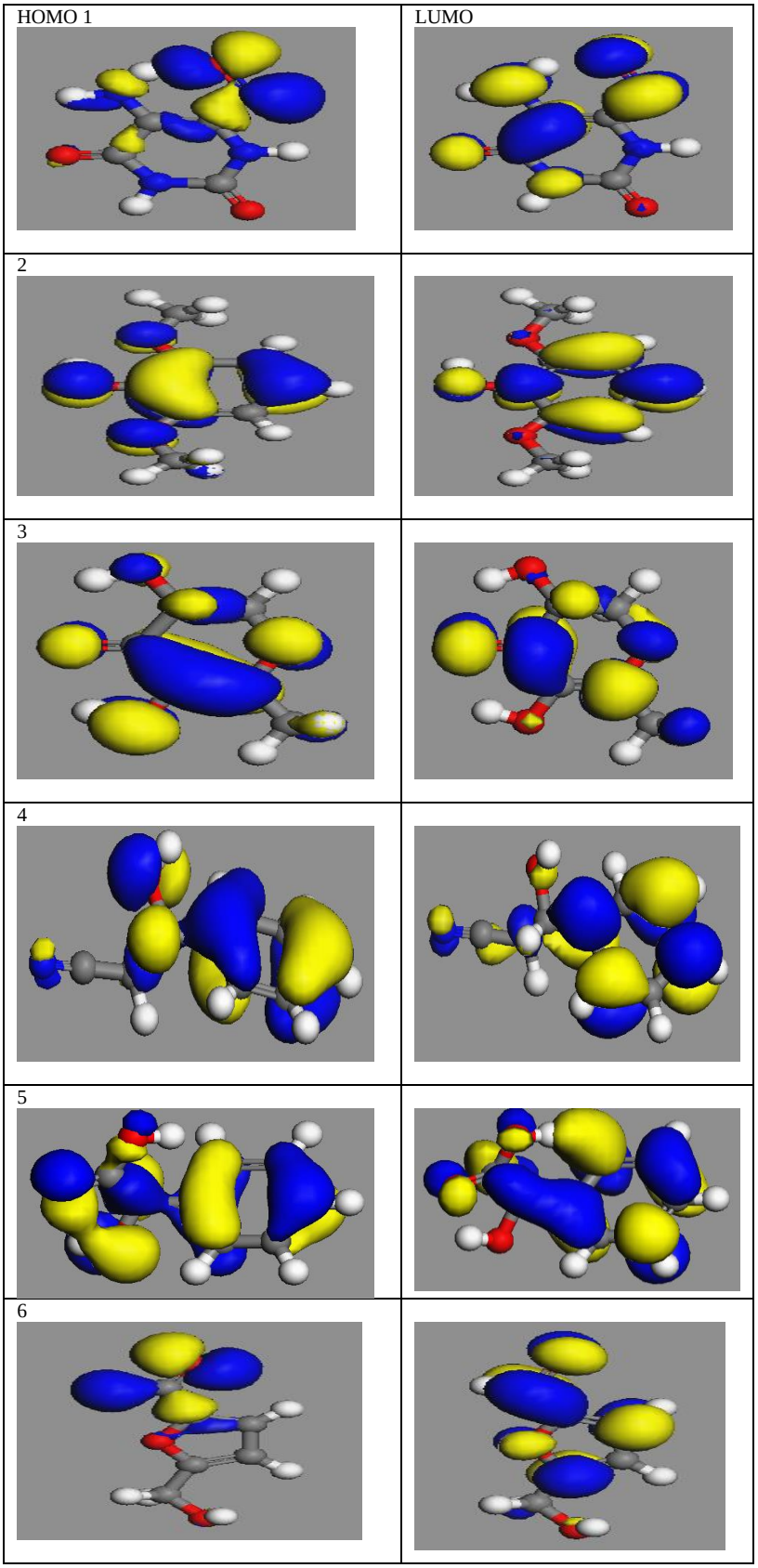

Figure 11: Frontier molecular orbital density distributions of six inhibitor molecules: HOMO (left); LUMO (right), 1 (PID), 2 (DOP), 3 (HPO), 4 (BPN), 5 (BAA), 6 (FCA)

Thermodynamic consideration

Thermodynamic functions for dissolution of FE164531 in 2 M HCl in the absence and presence of various concentrations of VD were obtained by applying the transition state Equation 7.

$$CR = \left(\frac{RT}{Nh}\right) exp\left(\frac{\Delta S_{ads}}{R}\right) exp\left(\frac{\Delta H_{ads}}{RT}\right) \quad (7)$$

Here in, *CR* is corrosion rate, *N* is Avogadro's number, *h* is plank's constant, *T* is absolute temperature and *R* is universal gas constant. Figure 10 depicts a plot of log (CR/T) *vs.* T^{-1}, which gave linear plots with slope of (-Δ*H**/2.303.R) and intercept of [Log(R/N.h)+(Δ*S*/2.303.R)] from which the values of Δ*H** and Δ*S** were evaluated. Data obtained indicates that the VD leaves extract acted through adsorption on FE164531 which barricades available corrosion active sites on the metal surface. Table 1 shows the values obtained for enthalpy of activation and entropy of activation for the dissolution and inhibition of FE164531 in 2 M HCl solution. The enthalpy of activation (ΔH*) values in the presence of VD leaves extract are higher than the value obtained in the absence of VD. The positive sign of ΔH* shows the endothermic nature of the process suggesting increase in temperature increases dissolution and retards inhibition efficiency. This agrees with the weight loss results that gave higher corrosion rates and decreased inhibition efficiency with increase in temperature. The entropy of activation (ΔS*) values were negative indicating a spontaneous process of dissolution and the adsorption process occurred in an orderly fashion on the FE164531 surface [33]. This signifies that the activated complex in the rate determining step represents association rather than dissociation, which enacted a decrease in disordering going from reactants to the activated complex. The opposite signs of ΔH_{ads} and ΔS_{ads} obtained for the corrosion process and its control could be seen as a cooperative effective rather than complimentary.

Quantum chemical calculations

Quantum chemical calculations and molecular dynamics studies were applied on PID, DOP, FCA, HPO, BPN and BAA to investigate their possible role as corrosion inhibitors for metal surfaces in acidic media. Existence of unique atoms like N, O and S in heterocyclic compounds has been widely reported as an effective parameter in improvement of inhibitor efficiency in acidic media [13-17,34]. The selection of potential corrosion inhibitor takes into consideration the geometric and electronic properties of molecules.

The molecules' geometry has strong influence on the adsorption behaviour of inhibitors on metal surface as it informs of the optimal orientation by which the inhibitor might cover the metal surface. Molecules with planar geometry have been reported to exhibit higher inhibition efficiency than corresponding compounds with less planar geometry [35]. Electronic parameters give insight about the molecules' tendency to react via donation/backdonation of electrons between the molecule and metal surface. However, such interactions depend strongly on the electron density distribution of molecule [34]. Regions that have high electron density would preferably undergo donate/accept electrons transfer with partially filled or vacant *d* orbital of the metal resulting in a donor-acceptor bond. Figure 11 illustrates the frontier molecular orbital density distribution showing HOMO and LUMO orbital while their energy values are listed in Table 3. According to Xia et al. [36], low lying LUMO induces a backdonation of charge from the metal to the molecule whereas high E_{HOMO} facilitates adsorption by influencing the transport process through the adsorbed layer. Herrag et al. [37] reported that excellent corrosion inhibitors are usually molecules that not only offer electrons to unoccupied orbital of the metal but also accept free electrons from the metal using their anti-bond orbital to form stable chelates. Analyzing the HOMO orbital of the inhibitor molecules, we observed that the HOMO orbital of PID molecule were found chiefly at the nitro N2, O8 group but had modest electric density at amine N11 group. This kind of orbital distribution could be ascribed to p-π conjugation effect, consideration the lone pair electrons and double bond at N2=O8. N11 had high charge population distribution (Table 3) attributed to the polarization of amine groups in acidic media. The LUMO orbital of PID were found at the same sites as the HOMO but with the inclusion of O7, N9 and C3-C6 bond hence, formation of a coordinate bond during adsorption which protects the metal and reduce the inherent reactivity of the metal at the sites where they are attached.

The HOMO orbital of DOP had electric density chiefly at C2-C1=C6 bond, at O7 atom and methoxy O8, O10 group while its LUMO orbital were delocalized within the hetero ring. Examination of the HOMO and LUMO orbital, DOP reveals formation of a donor/acceptor bond with the metal surface, however, considering the E_{LUMO} values in Table 3, the low value obtained for DOP showed the molecule to be of more electron acceptor. This indicates that DOP is preferably adsorbed on the iron surface by electron acceptance, that is, chemisorption by backdonation, rather than by donation of p-electrons to the metal. BAA has its HOMO orbital distributed around the molecule but chiefly on carbonyl group and along the hydrogen bond between O10 and O11 atom. The unshared electron pair on the oxygen atoms are weakly basic and can be protonated in acidic media, suggesting that the molecule will be attached at the cathodic site. We examined the LUMO orbital of BAA which had electric density delocalized at the π-bonding electrons of heterocyclic rings and non-bonding electrons pairs of O9 and O11 atom. The formation of adsorbed layer due to electrostatic interaction at the metal/electrolyte interface arises from the molecules' electron density which essentially blocks cathodic reaction and reduced anodic dissolution of the metal. This electrostatic interaction which is weak in nature supports the physical adsorption proposed by the weight loss results. The electric density for HOMO and LUMO plots of BPN were seen distributed around the hetero ring and small density at the nitrile N11 atom OEO had the HOMO and LUMO electric density at O9, methoxy O10 group and C1=C2, C3-C8 bond.

This indicates the sites with which the inhibitor molecules donate/accept electrons with the metal surface. The value is low whole the is high supporting that the molecule adsorbs by coordinate bond via electrostatic interaction. HPO had HOMO orbital chiefly at the C1-C2=C3 bond and also at O7, hydroxyl O8, O10 atom as a result of conjugate p-π contribution. The resonance within the hetero ring is assumed to engage the lone pair electrons on O4 thereby decreasing probable formation of coordinate bond despite the high population charge distribution. The π electrons of C1=O7 bond is assumed to move to the oxygen atom due to its electronegative, can easily accommodate negative charges acquired. The LUMO plot is observed to be around the hetero ring and O7 excluding the hydroxyl O8 and O10 atom.

However, considering the pollution charge distribution, the hydroxyl atoms carry high negative charges which are assumed to partake in the donor/acceptor bond with the metal surface. The HOMO plot of FCA is found at O7 while the LUMO plot was delocalized within the molecule. This indicates that FCA has only one adsorption center with which it can interact with the metal surface. Considering the HOMO and LUMO plots for the selected inhibitor molecules along with the Fukui functions, it can be inferred that inhibitor molecules investigated in this study were electron acceptors and the iron surface was the donor.

Table 3: Quantum chemical parameters of the inhibitor molecules calculated from gas phase

	f^-	f^+	Mulliken atomic charges	$-E_{HOMO}$ (eV)	$-E_{LUMO}$ (eV)	ΔE (eV)	E_{Bind} (kcal/mol)
PID	N(2) 0.011	N(2) 0.015	N(2) -0.412	5.5076	4.4763	-1.0313	-94.07
	O(7) 0.085	O(7) 0.097	O(7) -0.415				
	O(8) 0.087	O(8) 0.087	O(8) -0.419				
	O(10) 0.194	O(10) 0.158	O(10) -0.391				
	N(11) 0.083	N(11) 0.091	N(11) -0.394				
DOP	C(1) 0.070	C(1) 0.104	C(1) 0.223	4.8845	0.6531	-4.2314	-93.36
	O(7) 0.130	O(7) 0.066	O(7) -0.423				
	O(8) 0.035	O(8) 0.022	O(8) -0.484				
	O(10) 0.066	O(10) 0.031	O(10) -0.413				
BPN	C(2) 0.040	C(2) 0.069	C(2) -0.118	6.6205	1.7824	-4.8381	-87.41
	C(4) 0.059	C(4) 0.063	C(4) -0.099				
	C(6) 0.039	C(6) 0.048	C(6) -0.121				
	O(8) 0.118	O(8) 0.023	O(8) -0.465				
	N(11) 0.081	N(11) 0.080	N(11) -0.227				
BAA	C(4) 0.048	C(4) 0.023	C(4) -0.092	6.4573	2.1742	-4.2831	-88.06
	C(6) 0.013	C(6) 0.068	C(6) -0.194				
	O(9) 0.056	O(9) 0.047	O(9) -0.382				
	O(10) 0.161	O(10) 0.025	O(10) -0.484				
	O(11) 0.122	O(11) 0.088	O(11) -0.400				
HPO	O(4) 0.100	O(4) 0.066	O(4) -0.410	5.5647	2.8953	-2.6694	-78.76
	O(7) 0.101	O(7) 0.148	O(7) -0.474				
	O(8) 0.163	O(8) 0.053	O(8) -0.471				
	O(10) 0.058	O(10) 0.046	O(10) -0.484				
FCA	O(1) 0.025	O(1) 0.050	O(1) -0.363	5.992	2.966	-3.026	-73.62
	C(3) 0.037	C(3) 0.021	C(3) -0.157				
	O(7) 0.274	O(7) 0.158	O(7) -0.371				
	O(9) 0.043	O(9) 0.029	O(9) -0.489				

Local selectivity

Inhibition efficiency of compounds is closely related to the reactivity of individual molecular orbital contributions to the response of the whole molecular continuum. Condensed Fukui functions distinguish each part of the molecule on the basis of its distinct chemical behavior due to the different substituent functional groups [38]. The local reactivity of inhibitor molecules were analyzed by means of the condensed Fukui function and reported in Table 3. The site for nucleophilic attack will be the place where the value of $f+$ is the maximum while possible sites for electrophilic attack is controlled by high values of $f-$. Perusal of Table 3 revealed that the most reactive sites of PID are at O8, O10 atom for a coordinate bond formation. The Mulliken charge distribution presented in Table 3 shows that N2, O7 atom carry negative charged centers which might accept/donate electrons to the Fe surface to form coordinate bonds. DOP exhibited the propensity to donate electrons at O7 atom while the possibility of backdonation at C1 atom. The population analyses showed that O7, O8, O10 atom carries high negative charge indicating their participation in forming coordinate bonds. Analyzing the results obtained for BAA showed higher tendency to donate electrons than accept at O10, O11 atom. BPN and HPO showed the same trend at O8, N11 atom and O4, O7, O8 atom respectively. However, HPO showed propensity to accept electrons at O7 atom, thus forming a backdonation coordinate bond. BPN and BAA could accept electrons at N11 atom and O11 atom respectively. This indicates that the studied inhibitor molecules tend to adsorb on Fe surface via electron donation which supports the physical adsorption suggested by weight loss results. Results for Fukui function support the trend of the frontier molecular orbital observed for the studied molecules indicating the zones through which the molecule will be adsorbed onto the Fe(110) surface.

Molecular dynamics

To quantitatively evaluate the most suitable adsorption modes between each molecule and Fe(110) surface, the adsorption energy (E_{Bind}) was calculated using the relationship in Equation 5. In each case the potential energies were calculated by averaging the energies of five structures of the global minimum [18]. The obtained values are shown in Table 3 with PID exhibiting the highest binding energy during the simulation process. The high values of binding energy for PID could be attributed to its planar geometry and electronic properties. The unshared electron pair on the nitrogen (N4, N9) atoms is assumed to delocalize as part of the π aromatic system, enhancing electrostatic interaction with the metal surface. Further, the p-π conjugation system at O7, O8 atom results in dissociative adsorption which is favourable to crack the intramolecular bond of the adsorbate molecule [22].

The amine group is easily protonated in acidic media which suggests that the molecule is attached at the cathodic site, hence supporting the data from polarization experiment. From the high values of E_{Bind} obtained for PID, only a probable chemisorption is expected which affirms the observed electron acceptance and backdonation of electrons at the same site. DOP showed good binding energy which point to lone pair electrons on O atoms providing electrons to the unfilled *3d* orbital of iron surface thereby forming a protective layer. Such protective film may act as a steric barrier that hinders the reactive ions/species from corrosive environment, coming in contact with the metal surface thereby, slowing down corrosion process. FCA exhibited the least binding energy which shows that the five member ring has low inhibition efficiency than the six member ring. The low E_{Bind} is attributed to few reactive sites within the molecule available for interaction with the metal surface. Figure 12 show snapshots of the side view and top view (inset) of the lowest energy adsorption configurations for single inhibitor molecule simulated on the Fe(110) surface. Close inspection reveals a very clear fashion in the adsorption orientation of all inhibitor molecules, wherein polarizable atoms in the molecular backbone align with vacant sites on the fcc lattice atop the metal surface and virtually avoid contact with the Fe atoms along surface plane.

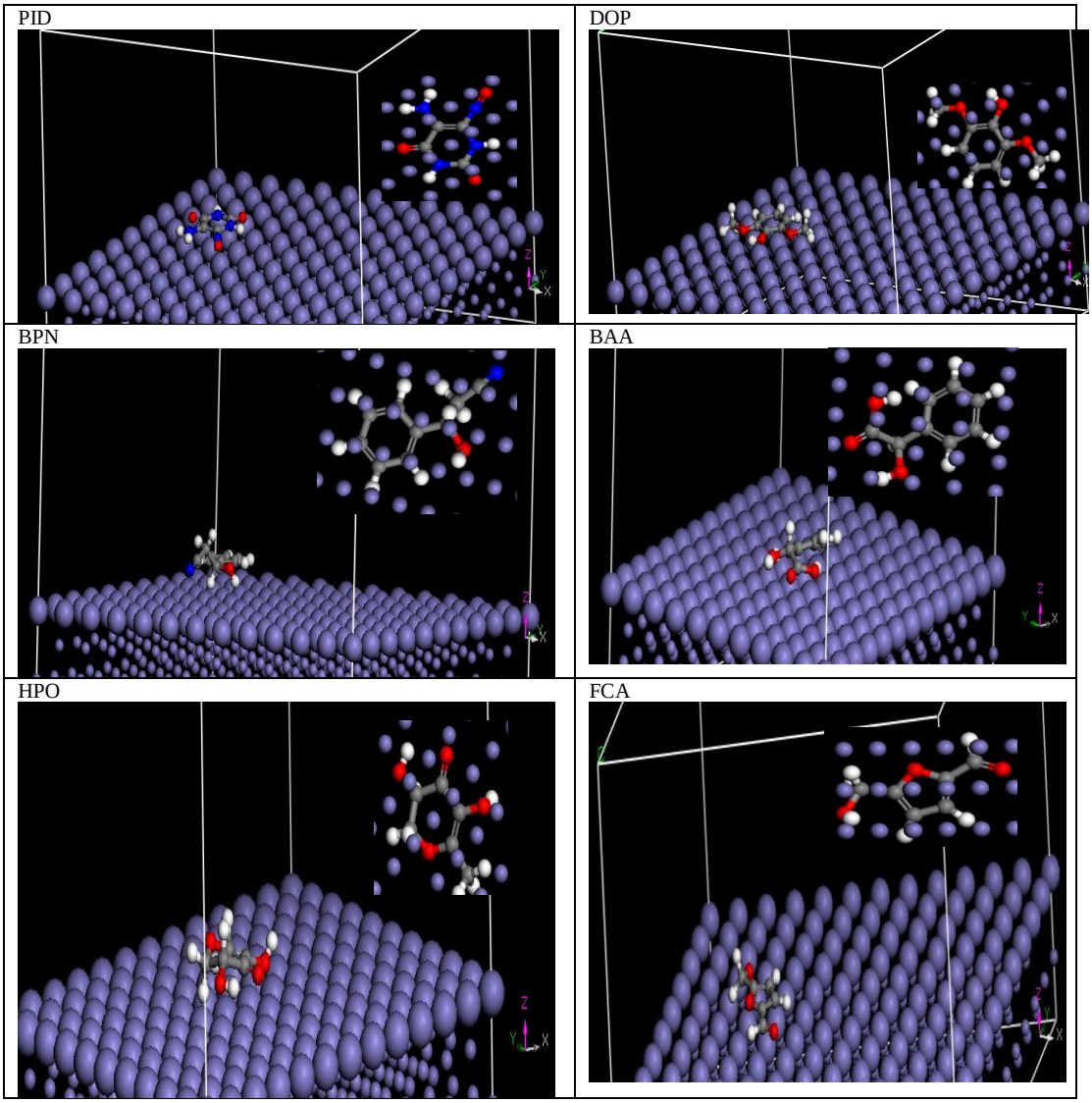

Figure 12: Representative snapshots of inhibitor molecules adsorbed on fcc lattice of Fe(110). Inset images show the on-top views

CONCLUSION

The presence of *V. doniana* leaves extract in 2 M HCl solution for FE164531 carbon steel corrosion inhibition remarkably shifted the values of E_{corr} to the less negative direction as well as decreased the values of i_{corr}. These were confirmed by the impedance results where the effect of inhibitor addition is distinguished by increased value in charge transfer resistance and a reduction of CPE values. The obtained IE% increased with increase in inhibitor concentration, suggesting greater molecular adsorption at active sites on FE164531 surface and a decrease in corrosion rate. Increase in experimental temperature decreased IE% which proposed a physical adsorption of VD leaves extract, suggesting a reduction in the time lag between adsorption and desorption of inhibitor molecules. Quantum chemical calculations show that VD molecules adsorbed directly at the metal/electrolyte interface by donor–acceptor interactions between π electrons of heterocyclic ring, nonbonding lone pairs of O and N atoms and vacant *d*-orbital of Fe atoms. Condensed Fukui functions demonstrate the nucleophilic and electrophilic attacking sites of the VD molecules. The population (Mulliken) charge distribution showed that the inhibitor molecules had better tendency to accept electrons from the metal surface.

REFERENCES

[1] M. Özcan, F. Karadağ, I. Dehri, *Acta. Phys. Chim. Sin.*, **2008**, 24(8), 1387-1392.
[2] L. Niu, H. Zhang, F. Wei, S. Wu, X. Cao, P. Liu, *J. Appl. Surf. Sci.*, **2005**, 252(5), 1634-1642.
[3] A.Y. El-Etre, M. Abdallah, Z.E. El-Tantawy, *Corros. Sci.*, **2005**, 47(2), 385-395.
[4] P Bothi-Raja, M.G. Sethuraman, *Mater. Corros.* **2009**, 60, 22-28.
[5] A.M. Abdel-Gaber, B.A. Abd-El-Nabey, M. Saadawy, *Corros. Sci.*, **2009**, 51, 1038-1042.
[6] G. Song, A. Atrens, D. St John, X. Wut, *J. Nairn, Corros. Sci.*, **1997**, 39(10-11), 1981-2004.
[7] E.O. Emeka, *Chem. Eng. Comm.*, **2009**, 196(5), 591-601.
[8] I. Ahamad, R. Prasad, M.A. Quraishi, *Mater. Chem. Phys*., **2010,** 124, 1155-1165.
[9] I. Ahamad, R. Prasad, M.A. Quraishi, *Corros. Sci.*, **2010**, 52, 3033-3041.
[10] J. Aljourani, K. Raeissi, M.A. Golozar, *Corros. Sci*., **2009**, 51, 18360-1843.
[11] S. Deng, X. Li, H. Fu, *Corros. Sci.*, **2010**, 52, 3840-3846.
[12] H. Ju, Z.P. Kai, Y. Li, *Corros. Sci*., **2008**, 50, 865-871.

[13] P. Zhao, Q. Liang, Y. Li, *Appl. Surf. Sci*., **2005**, 252, 1596-1607.
[14] M. Lebrini, M. Traisnel, M. Lagrenée, B. Mernari, F. Bentiss, *Corros. Sci*., **2008**, 50, 473-479.
[15] F. Bentiss, B. Mernari, M. Traisnel, H. Vezin, M. Lagrenée, *Corros. Sci*., **2010**, 53, 487-495.
[16] K.F. Khaled, *Corros. Sci*., **2010**, 52, 3225-3234.
[17] E.E. Oguzie, S.G. Wang, Y. Li, F.H. Wang, *J. Phy. Chem. C.*, **2009**, 113, (19) 8420-8429.
[18] O. Ladeji, Z.S.C. Okoye, *Pharm. Biol.*, **1996**, 34(5), 355-358.
[19] S. John, B. Joseph, K.V. Balakrishnan, K.K. Aravindakshan, A. Joseph, *Mater. Chem. Phy.*, **2010**, 123, 218-224.
[20] L.M. Rodrıguez-Valdez, A. Martınez-Villafane, D. Glossman-Mitnik, *J. Mol. Struct: Theochem.*, **2005**, 713(1–3), 65-70.
[21] A. Lesar, I. Milosev, *Chem. Physics. Letter*., **2009**, 483(4-6), 198-203.
[22] R.S. Oguike, A.M. Kolo, A.M. Shibdawa, H.A. Gyenna, *Physical. Chem.*, **2013**, 175910, 1-9.
[23] R.S. Oguike, *Adv. Mater. Phy. Chem*., **2014**, 4, 153-163.
[24] A.I. Onuchukwu, *Mater. Chem. Phy.*, **1990**, 337-341
[25] S. Zhang, Z. Tao, W. Li, B. Hou, *Appl. Surf. Sci*., **2009**, 255, 6757-6763.
[26] M. Scendo, *Corros. Sci*., **2007**, 49, 373-390.
[27] L.M. Rivera-Grau, M. Casales, I. Regla, D.M. Ortega-Toledo, *Int. J. Electrochem. Sci.*, **2013**, 8, 2491-2503.
[28] D. Wanga, S. Lia, Y. Yinga, M. Wanga, H. Xiaob, Z. Che, *Corros. Sci.*, **1999**, 41(10), 1911-1919
[29] M. Behpour, S.M. Ghoreishi, M. Salavati-Niasari, B. Ebrahimi, *Mater. Chem. Phys.*, **2008**, 107, 153-157.
[30] J. Bartley, N. Huynh, S.E. Bottle, H. Flitt, T. Notoya, D.P. Schweinsberg, *Corros. Sci.*, **2003**, 45(1), 81-96.
[31] I.O. Arukalam, I.C. Madufor, O. Ogbobe, E.E. Oguzie, *British J. Appl. Sci. Tech.*, **2014**, 4(9), 1445-1460.
[32] B.I. Ita, C.A. Edem, *Global Journal of Pure Applied Sciences*, **2000**, 60(20), 239-252.
[33] M.A. Amin, K.F. Khaled, Q. Mohsen, H.A. Arida, *Corros. Sci*., **2010**, 52, 1684-1695.
[34] F. Kandemirli, S. Sagdinc, *Corros. Sci*., **2007**, 49(5), 2118-2130.
[35] E.E. Ebenso, T. Arslan, F. Kandemirli, I. Love, C. Ogretir, M. Saracoglu, S.A. Umoren, *Theoret. Inter. J. Quantum. Chem*. **2010**, (110), 2614-2636
[36] S. Xia, M. Yu, L. Liu, F. Zhao, *Corros. Sci.*, **2008**, 50(7), 2021-2029.
[37] L. Herrag, B. Hammouti, S. Elkadiri, A. Aouniti, C. Jama, H. Vezin, F. Bentiss, *Corros. Sci*., **2010**, 52, 3042-3051.
[38] K.F. Khaled, N.S. Abdel-Shafi, N.A. Al-Mobarak, *Int. J. Electrochem. Sci.*, **2012**, 7, 1027-1044.